Compound Radiating Slots in a Broad Wall of a Rectangular Waveguide

SEMBIAM R. RENGARAJAN, SENIOR MEMBER, IEEE

Abstract—**An analysis is presented of the characteristics of a broad wall radiating slot, offset from the center line and tilted with respect to the longitudinal axis of a rectangular waveguide. Pertinent integral equations are developed, taking into account finite wall thickness, and are solved for the slot aperture *E*-field using the method of moments. Compound slot characteristics are then deduced, including resonant length, and dominant mode scattering. Numerical results for the scattering from resonant slots are presented over a range of offsets, tilt angles, frequencies, and waveguide dimensions. For resonant compound slots, offset and tilt are shown to control the aperture electric field amplitude with a phase variability of 360°. Results presented in this paper have significant applications in the design of compound slot arrays.**

I. Introduction

THE IMPORTANCE of the broad wall compound slot can be appreciated by comparing it to the centered-inclined radiating slot, and to the longitudinal offset slot, shown in Fig. 1. For a resonant length, centered-inclined slot, the phase of the electric field in the slot referenced to the phase of the incident TE_{10} mode which excites the slot is 0° for $0 \le \theta \le 90°$ and 180° for $-90° \le \theta \le 0°$. The amplitude of the field depends on the amount of tilt. For a resonant length longitudinal slot, the phase of the electric field in the slot is 90° for $\delta > 0$ and 270° for $\delta < 0$. The amplitude of the field depends on the amount of offset. For a resonant length compound slot, the phase of the electric field in the slot can have *any value between 0 and 360°* depending on offset and tilt, as depicted in Fig. 2. The amplitude of the field depends on both offset and tilt. This property of the compound slot was first noticed by Maxum [1] who employed this element in an antenna array. The versatility of the compound slot is well suited to the design of a fuze antenna for missile applications, where one needs to place the main beam from a linear array at some arbitrary angle off the nose direction. Control of the uniform progressive phase in the aperture distribution is easily achieved with compound slots.

Stevenson formulated the general broad wall slot problem in the form of an integral equation in terms of waveguide and free space Green's functions [2]. He also obtained approximate expressions for the scattering off resonant slots. Watson derived equivalent circuit representations using a transmission line analogy [3]. Recently, Elliott developed an iterative technique to design small slot arrays of longitudinal elements [4]. This procedure requires a knowledge of the scattering property of a single slot as a function of slot length and offset, since this information is used to "detune" the slot to compensate for mutual coupling. A compound slot array can be designed using a modified Elliott's procedure (with scattering wave representation of the slots) by keeping all elements resonant and using offset and tilt as the control parameters.

The longitudinal slot in the broad wall of a rectangular waveguide has been successfully analyzed by the method of moments [5]–[7]. The analysis of a compound slot is more involved and hence, in the past, the design of compound slot arrays relied on experimentally obtained data. An experimen-

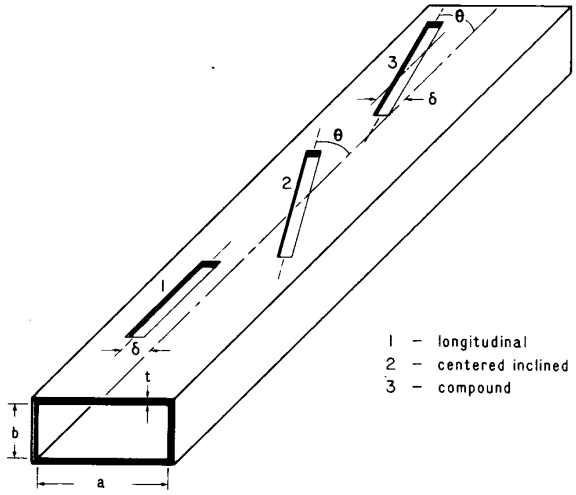

Fig. 1. Broad wall radiating slots.

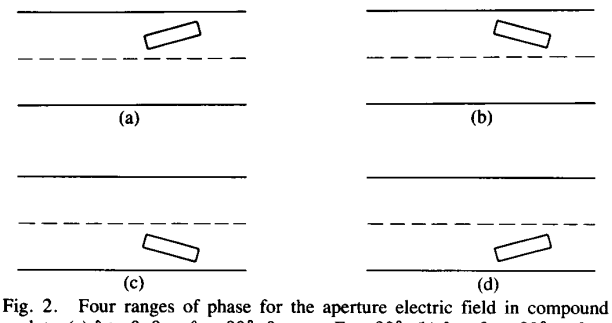

Fig. 2. Four ranges of phase for the aperture electric field in compound slots. (a) $\delta > 0, 0 \le \theta \le 90°, 0 \le \arg E \le 90°$. (b) $\delta > 0, -90° \le \theta \le 0, 90° \le \arg E \le 180°$. (c) $\delta < 0, -90 \le \theta \le 0, 180° \le \arg E \le 270°$. (d) $\delta < 0, 0 \le \theta \le 90°, 270° \le \arg E \le 360°$.

Manuscript received May 18, 1988; revised November 18, 1988. This work was supported by the Hughes Aircraft Company and the University of California, Los Angeles.

The author was with the University of California, Los Angeles, on leave from the Department of Electrical and Computer Engineering, California State University, Northridge, CA 91330.

IEEE Log Number 8927849.

0018-926X/89/0900-1116$01.00 © 1989 IEEE

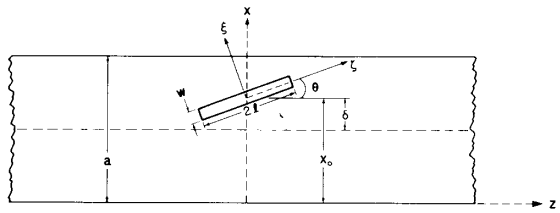

Fig. 3. Geometry of a compound slot.

tal difficulty arises in attempting to determine the resonant length of a compound slot as a function of its offset and tilt, since resonance is defined by the condition that the forward scattered TE_{10} mode be out of phase with the incident TE_{10} mode [1], [3]. Forward scattering is difficult to measure, even on a modern automatic network analyzer; this problem is exacerbated if the waveguide is dielectric-filled, as is commonly the case. Thus a strong need exists for finding a theoretical way to determine the characteristics of the compound slot so as to avoid costly experimental data taking. This paper fills such a need, and also helps to provide a better understanding of the compound slot.

II. Analysis

A. The Integral Equations

Fig. 3 shows the geometry of a compound radiating slot cut in the upper broad wall of an infinitely long rectangular waveguide. The broad wall containing the slot is assumed to be embedded in a perfectly conducting ground plane of infinite extent. The waveguide is completely filled with a linear isotropic lossless dielectric whose constitutive parameters are μ_0, and ϵ. The outer half-space is assumed to be a vacuum. Schelkunoff's equivalence principle is invoked to divide the original problem into three regions. Region 1 is the waveguide interior, with the slot completely shorted and a magnetic current placed in its location. The magnetic current is $\bar{K}_m^{(1)} = \hat{y} \times \bar{E}_a^{(1)}$ where $\bar{E}_a^{(1)}$ is the interior aperture electric field. It is assumed that the slot width w is very much less than slot length $2l$. This assumption justifies neglecting the longitudinal component of the electric field [5]–[7]. Thus $\bar{E}_a^{(1)} = \hat{\xi}\, E_{a\xi}^{(1)}$. Region 3 is the outer half-space bounded by the infinite ground plane, with the slot aperture shorted, and a magnetic current placed in its location. This magnetic current is $\bar{K}_m^{(2)} = -\hat{y} \times \bar{E}_a^{(2)}$, where $\bar{E}_a^{(2)}$ is the exterior aperture electric field. Again $\bar{E}_a^{(2)} = \hat{\xi}\, E_{a\xi}^{(2)}$ since the longitudinal component of the electric field is ignored. Region 2 is a cavity, with both the interior and exterior slot apertures shorted and magnetic currents $-\bar{K}_m^{(1)}$ and $-\bar{K}_m^{(2)}$ placed in their locations, respectively. This cavity has cross-sectional dimensions $2l$, w and length t, which is the thickness of the top broad wall. A pair of coupled integral equations are obtained by enforcing the continuity of longitudinal magnetic fields across the interior and exterior slot apertures denoted by subscripts 1 and 2, respectively. These equations are

$$H_{\zeta i}^{-} = H_{\zeta i}^{+}; \qquad i = 1, 2. \tag{1}$$

The superscripts $-$ and $+$ refer to "just inside" and "just outside" each aperture, respectively. Equation (1) gives rise to

$$H_{\zeta 1}^{c} - H_{\zeta 1}^{\text{scat}} = H_{\zeta}^{\text{inc}} \tag{2a}$$

$$-H_{\zeta 2}^{c} + H_{\zeta 2}^{\text{ext}} = 0. \tag{2b}$$

H_{ζ}^{inc} is the longitudinal magnetic field in the interior slot aperture due to a TE_{10} mode waveguide source, given by

$$H_{\zeta}^{\text{inc}} = A_{10} e^{-j\beta_{10} z} \left[j \cos\left(\frac{\pi x}{a}\right) \cos\theta - \frac{\beta_{10}}{(\pi/a)} \sin\left(\frac{\pi x}{a}\right) \sin\theta \right] \tag{3}$$

where A_{10} is the amplitude and β_{10} is the propagation constant. Time dependence in the form $e^{j\omega t}$ is assumed. The left-side terms in the above equations involve the magnetic currents in the two apertures, $K_{m\zeta}^{(1)}$ and $K_{m\zeta}^{(2)}$ where $K_{m\zeta}^{(1)} = -E_{\xi}^{(1)}$ and $K_{m\zeta}^{(2)} = E_{\xi}^{(2)}$. $H_{\zeta 1}^{\text{scat}}$ is the longitudinal field in the interior aperture due to the magnetic current $K_{m\zeta}^{(1)}$ in the waveguide.

$$H_{\zeta 1}^{\text{scat}} = \iint_{S_1} [\cos\theta \sin\theta][G^{\text{scat}}] \begin{bmatrix} \cos\theta \\ \sin\theta \end{bmatrix} K_{m\zeta}^{(1)}\, ds'. \tag{4}$$

The integration is carried out over the interior slot aperture area S_1.

$$[G^{\text{scat}}] = \begin{bmatrix} G_{zz}^{\text{scat}} & G_{zx}^{\text{scat}} \\ G_{xz}^{\text{scat}} & G_{xx}^{\text{scat}} \end{bmatrix}$$

are Stevenson's Green's functions [2], [8].

$H_{\zeta 1}^{c}$ is the lower aperture field in the cavity due to the magnetic current sheets $-K_{m\zeta}^{(1)}$ and $-K_{m\zeta}^{(2)}$, i.e.,

$$H_{\zeta 1}^{c} = -\iint_{S_1} G_{s\zeta\zeta}^{c} K_{m\zeta}^{(1)}\, ds' - \iint_{S_2} G_{c\zeta\zeta}^{c} K_{m\zeta}^{(2)}\, ds' \tag{5}$$

where s_2 is the exterior slot aperture area, $G_{s\zeta\zeta}^{c}$ and $G_{c\zeta\zeta}^{c}$ are cavity region Green's functions. These are obtained from the corresponding waveguide Green's functions (treating y as the propagation direction) using the method of scattering superposition [9]. These Green's functions do not have any singular terms [10], and they are given by

$$G_{s\zeta\zeta}^{c} = \frac{2\omega\epsilon}{wlk^2} \sum_{m=1}^{\infty} \sum_{n=0}^{\infty} \frac{\epsilon_{mn}^2}{j\gamma'_{mn}} \left[k^2 - \left(\frac{m\pi}{2l}\right)^2 \right] \cdot f(\zeta, \zeta', \xi, \xi') \coth(\gamma'_{mn} t) \tag{6}$$

$$G_{c\zeta\zeta}^{c} = \frac{2\omega\epsilon}{wlk^2} \sum_{m=1}^{\infty} \sum_{n=0}^{\infty} \frac{\epsilon_{mn}^2}{j\gamma'_{mn}} \left[k^2 - \left(\frac{m\pi}{2l}\right)^2 \right] \cdot \frac{f(\zeta, \zeta', \xi, \xi')}{\sinh(\gamma'_{mn} t)} \tag{7}$$

where $f(\zeta, \zeta', \xi, \xi') = \sin(m\pi\zeta/2l) \cos(n\pi\xi/w) \sin(m\pi\zeta'/2l) \cos(n\pi\xi'/w)$ and $\gamma'_{mn} = [k^2 - (m\pi/2l)^2 - (n$

$\pi/w)^2]^{1/2}$ if γ'^2_{mn} is positive and $\gamma'_{mn} = j\beta'_{mn}$ when γ'^2_{mn} is negative. k is the wavenumber in the cavity region. In (6) and (7), $\epsilon^2_{00} = 1/4$, $\epsilon^2_{m0} = 1/2$, $\epsilon^2_{0n} = 1/2$, $\epsilon^2_{mn} = 1$, $m \neq 0$ and $n \neq 0$.

$H^c_{\zeta 2}$ is the upper aperture magnetic field in the cavity due to the magnetic current sheets $-K^{(1)}_{m\zeta}$ and $-K^{(2)}_{m\zeta}$, i.e.,

$$H^c_{\zeta 2} = -\iint_{s_1} G^c_{c\zeta\zeta} K^{(1)}_{m\zeta}\, ds' - \iint_{s_2} G^c_{s\zeta\zeta} K^{(2)}_{m\zeta}\, ds'. \tag{8}$$

$H^{\text{ext}}_{\zeta 2}$ is the upper aperture field in the half-space. Using the image principle, one finds that this field is given by

$$H^{\text{ext}}_{\zeta 2} = \iint_{s2} G^{\text{ext}}_{\zeta\zeta} K^{(2)}_{m\zeta}\, ds' \tag{9}$$

where $G^{\text{ext}}_{\zeta\zeta} = 1/j2\pi\omega\mu_0[\partial^2/\partial\zeta'^2 + k_0^2][e^{-jk_0R}/R]$, where k_0 is the free space wavenumber, and where $R = [(\zeta - \zeta')^2 + (\xi - \xi')^2]^{1/2}$. Use of (3)–(9) in (2) yields a pair of coupled integral equations in two unknowns, $K^{(1)}_{m\zeta}$ and $K^{(2)}_{m\zeta}$, which are surrogates for the aperture electric fields.

B. Method of Moments Solution of the Integral Equations

The integral equations (2) have been solved by the method of moments. For *longitudinal* slots, results obtained from two approaches are in excellent agreement with experimental data for the self-admittance and resonant length [7]. These two approaches used piecewise sinusoidal Galerkin and global sinusoidal Galerkin techniques, respectively, to obtain the longitudinal E-field distribution in the slot apertures. Both formulations employed a quasistatic transverse distribution for the slot aperture E-field in the form $[1 - (2\xi'/w)^2]^{-1/2}$, thereby enforcing edge conditions for thin wall slots. For *compound* slots, a piecewise sinuisoidal expansion is not convenient since it loses its Toeplitz property. Also, the global Galerkin technique has the advantage that a few expansion modes are usually adequate to insure a good solution near resonance. For a compound slot, employing edge singularities in the transverse distribution introduces additional summations and numerical integrations compared to a model which uses a uniform transverse distribution. Therefore a global Galerkin technique embodying pulse functions to represent transverse distribution has been employed in this work. This approach was previously applied to a longitudinal slot by Lyon and Sangster [6]. Thus it has been assumed that

$$K^{(1)}_{m\zeta}(\xi, \zeta) = \sum_{q=1}^{N} A_q \sin[q\pi(\zeta + l)/(2l)] \tag{10}$$

$$K^{(2)}_{m\zeta}(\xi, \zeta) = \sum_{q=1}^{N} B_q \sin[q\pi(\zeta + l)/(2l)] \tag{11}$$

are the global expansions. Here the A and B are the $2N$ unknown coefficients. A matrix equation of order $2N$ is obtained by taking inner products of each side of (2a) and (2b) with N testing functions of the form

$$w_p(\xi, \zeta) = \delta(\xi) \sin[p\pi(\zeta + l)/(2l)]. \tag{12}$$

The matrix equation is expressed in terms of partitioned matrices

$$\left[\begin{array}{c|c} [Y_{11}] & [Y_{12}] \\ \hline [Y_{21}] & [Y_{22}] \end{array}\right] \left[\begin{array}{c} A_1 \\ A_2 \\ \cdot \\ \cdot \\ \cdot \\ A_N \\ \hline B_1 \\ B_2 \\ \cdot \\ \cdot \\ \cdot \\ B_N \end{array}\right] = \left[\begin{array}{c} I_1 \\ \cdot \\ \cdot \\ \cdot \\ I_N \\ \hline 0 \\ 0 \\ \cdot \\ \cdot \\ \cdot \\ 0 \end{array}\right]. \tag{13}$$

Here

$$I_p = \int_{-l}^{l} \sin[p\pi(\zeta + l)/(2l)]\, H^{\text{inc}}_{\zeta}(\zeta, \xi = 0)\, d\zeta \tag{14}$$

and $[Y_{11}] = [Y^{\text{int}}] - [y^c_s]$ is an $N \times N$ matrix in which

$$Y^{\text{int}}_{p,q} = -\int_{-l}^{l} \sin[p\pi(\zeta + l)/(2l)] \cdot \iint_{s_1} [\cos\theta \ \sin\theta][G^{\text{scat}}] \left[\begin{array}{c} \cos\theta \\ \sin\theta \end{array}\right] \cdot \sin[q\pi(\zeta' + l)/(2l)]\, d\zeta'\, d\xi'\, d\zeta. \tag{15}$$

$[y^c_s]$ is a diagonal matrix where each element is

$$y^c_{sp,p} = \int_{-l}^{l} d\zeta \sin[p\pi(\zeta + l)/(2l)] \cdot \iint_{s_1} G^c_{s\zeta\zeta} \sin[q\pi(\zeta' + l)/(2l)]\, d\zeta'\, d\xi' = -j\frac{l}{\omega}\frac{\gamma'_{p0}}{\mu_0} \coth(\gamma'_{p0} t). \tag{16}$$

From (16) we find that each expansion mode, p excites only one evanescent mode TE_{p0} in the cavity region waveguide of cross section $2l \times w$. For $p = 1$, this becomes a propatating mode if $2l > \lambda/2$ where λ is the free space wavelength and

$$y^c_{s1,1} = -j\frac{l}{\omega}\frac{\beta'_{p0}}{\mu_0} \cot(\beta'_{p0} t). \tag{17}$$

Similarly $[Y_{12}]$ is also an $N \times N$ diagonal matrix where each element is

$$Y_{12p,p} = -j\frac{l}{\omega}\frac{\gamma'_{p0}}{\mu_0} [\sinh(\gamma'_{p0} t)]^{-1}. \tag{18}$$

If $2l > \lambda/2$, for $p = 1$, $\gamma'_{p0} = j\beta'_{p0}$.

$$[Y_{21}] = -[Y_{12}]. \tag{19}$$

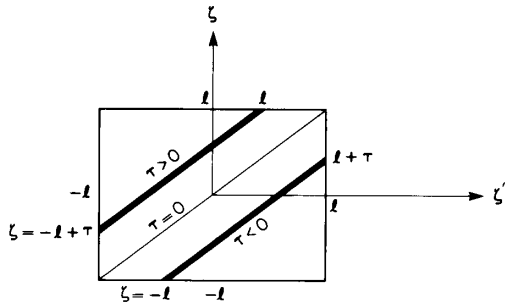

Fig. 4. Coordinate transformation.

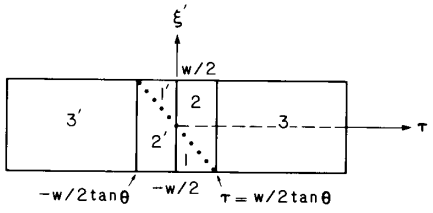

···· Singular region, z=z'

Fig. 5. Singular and nonsingular regions of Y_{pq}^{int}.

$[Y_{22}] = [Y^{\text{ext}}] + [y_s^c]$ is an $N \times N$ matrix in which

$$Y_{p,q}^{\text{ext}} = \int_{-l}^{l} \sin\left[p\pi(\zeta+l)/(2l)\right] \cdot \left[\iint_{S_2} G_{\zeta\zeta}^{\text{ext}} \sin\left[q\pi(\zeta'+l)/(2l)\right] ds'\right] d\zeta. \quad (20)$$

The external matrix elements are computed from (20). The differential operation in the Green's function in the above expression is simplified by integration by parts. The double integral in terms of longitudinal coordinates ζ and ζ' is reduced to a numerical single integral via a coordinate transformation, $\tau = \zeta - \zeta'$ as shown in Fig. 4. Thus

$$\int_{\zeta=-l}^{l} f_p(\zeta) \int_{\zeta'=-l}^{l} f_q(\zeta') \frac{e^{-jkR}}{R} d\zeta' \, d\zeta = \int_{\tau=0}^{2l} \frac{e^{-jkR}}{R} \int_{\zeta=-l+\tau}^{l} f_p(\zeta) f_q(\zeta-\tau) \, d\zeta \, d\tau + \int_{\tau=-2l}^{0} \frac{e^{-jkR}}{R} \int_{\zeta=-l}^{l+\tau} f_p(\zeta) f_q(\zeta-\tau) \, d\zeta \, d\tau. \quad (21)$$

In (21), the ζ integrals involve trigonometric functions f_p and f_q, and they are solved analytically. The remaining double integral in (20) is evaluated numerically. The use of symmetry considerations makes the computational time for $Y_{p,q}^{\text{ext}}$ proportional to N, instead of N^2.

Because of the complexity of the internal matrix elements $Y_{p,q}^{\text{int}}$, given by (15), the compound slot problem proved to be an order of magnitude more difficult to solve than the longitudinal slot problem [7]. The coordinate transformation employed for the external matrix elements helps in separating the singular region contributions to the internal matrix elements. Additionally, the presence of odd and even symmetries in regions 1, 1', 2, 2' and 3, 3' in Fig. 5 is exploited in the algebraic simplification. As shown in Fig. 5,

$$z - z' = (\zeta - \zeta')\cos\theta - (\xi - \xi')\sin\theta = \tau\cos\theta + \xi'\sin\theta, \qquad \text{since } \xi = 0.$$

The singular region is given by $z = z'$ or $\tau = -\xi' \tan\theta$. The singular contribution is in the form of an integral

$$\int_{\zeta=-l}^{l} \int_{\zeta'=-l}^{l} \int_{\xi'=-w/2}^{w/2} f(\zeta, \zeta', \xi')\delta(z-z') \, d\zeta \, d\zeta' \, d\xi' = \int_{\xi'=0}^{w/2} \int_{\zeta=-l}^{l-\xi'\tan\theta} f(\zeta, \zeta+\xi'\tan\theta, \xi') \frac{1}{\cos\theta} d\zeta \, d\xi' + \int_{-w/2}^{0} \int_{-l-\xi'\tan\theta}^{l} f(\zeta, \zeta+\xi'\tan\theta, \xi') \frac{1}{\cos\theta} d\zeta \, d\xi'.$$

Here $\tan\theta$ is assumed positive and the expression $1/\cos\theta$ is the Jacobian associated with the integration in ζ, ξ' coordinates for the singular region. Nonsingular region contributions to $Y_{p,q}^{\text{int}}$ in (20) are in terms of integrals involving exponential and trigonometric functions and these are carried out analytically. However, this analysis requires considerable algebraic manipulation and results in a double summation, containing numerous expressions [11]. Because of space constraints the $Y_{p,q}^{\text{ext}}$ and $Y_{p,q}^{\text{int}}$ expressions are not presented in this paper. The double summations in $Y_{p,q}^{\text{int}}$ exhibit slow convergence, and hence evaluation of $Y_{p,q}^{\text{int}}$ takes most of the computer time in compound slot calculation. The aperture electric field is determined from a solution of (13). The dominant mode scattering in the waveguide is then computed using Stevenson's Green's function for the TE_{10} mode.

III. Numerical Results and Discussion

At resonance, forward and backward scattered TE_{10} mode amplitudes are the same for compound slots. The aperture electric field phase is half the TE_{10} mode backscattered wave phase, both referenced to the incident TE_{10} mode at the center of the slot. Over a small frequency range off resonance, the phases of forward and backward scattered waves and that of the aperture electric field very nearly track each other. The resonant length, aperture electric field magnitude, and forward and backscattered wave amplitudes are dependent on the magnitude of offset δ and tilt θ. When one or both of these quantities is negative, the aperture electric field phase is obtained from the corresponding value of a slot having positive θ and δ, based on symmetry considerations shown in Fig. 2. Therefore all the results discussed below pertain to the resonant slot orientation shown in Fig. 2(a) with positive values for δ and θ.

A. Resonant Length

Fig. 6 and 7 illustrate the normalized resonant length $2k_0 l$ as a function of slot offset δ. It is found that the resonant length is

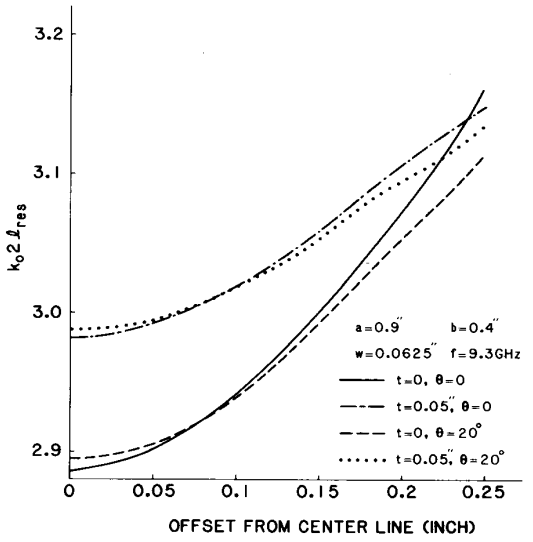

Fig. 6. Resonant length of compound slots for a standard X-band waveguide.

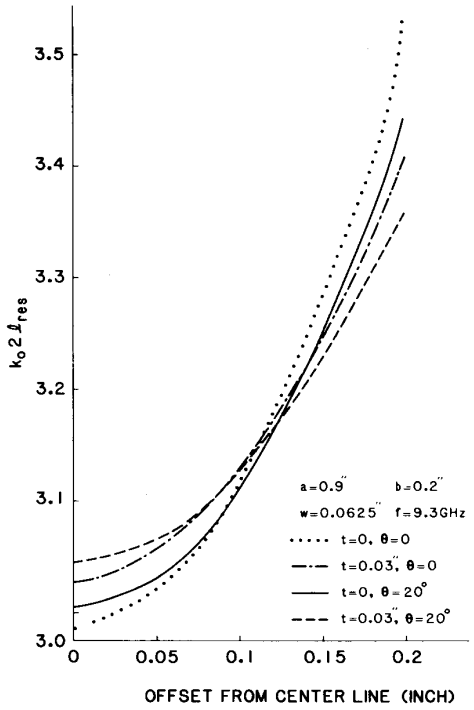

Fig. 7. Resonant length of compound slots for a half-height guide.

primarily dependent on δ, and that it is essentially insensitive to the tilt θ for $0 < \theta < 20°$. For a thick wall slot, resonant length increases with wall thickness, t if $2l < \lambda/2$ where λ is the free space wavelength. When $2l > \lambda/2$, the resonant length decreases with t. This behavior can be explained from a transmission line analogy by considering only one mode between the upper and lower slot apertures. Previously such results were reported for longitudinal slots [12], [5], [6]. At present, compound slot array designs are based on the assumption that the resonant length is independent of tilt angle. This assumption generally proves to be correct for slots in a

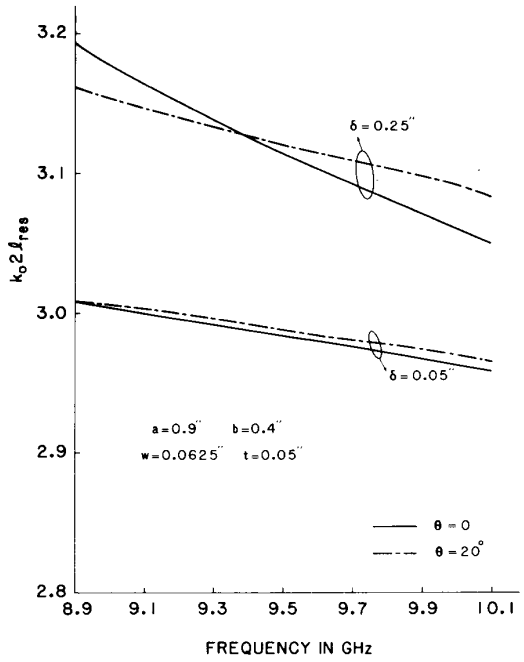

Fig. 8. Resonant length versus frequency for a standard X-band guide.

standard height X-band waveguide. However, for reduced height waveguides, especially for larger offsets, the change in resonant length becomes significant, even for thick wall slots. It is interesting to note that for very small offsets, where the slot is predominantly a series element, resonant length increases with θ, whereas for larger offsets, where the shunt effect dominates, resonant length decreases with θ. Maxum's experimental results do not show the correct behavior for larger offsets [1]. Fig. 8 shows the normalized resonant length for a frequency range of 8.9 to 10.1 GHz. For a 50 mil thick wall standard X-band guide, the resonant length decreases by 1.7 percent for $\theta = 0$ and 1.5 percent for $\theta = 20°$ when $\delta = 50$ mil. These figures are substantially larger (4.5 and 2.5 percent) for a 250 mil offset. Thus there is a need to compute the resonant length accurately at the design frequency, taking both δ and θ into account.

B. The Backscattered Wave Amplitude $|s_{11}|$

Figs. 9 and 10 exhibit the magnitude of the backscattered wave, $|s_{11}|$ as a function of δ for standard height and half-height X-band waveguides at resonance. For small offsets, $|s_{11}|$ varies very rapidly as a function of θ, while for large offsets $|s_{11}|$ is relatively insensitive to θ. $|s_{11}|$ is larger for reduced height waveguides, as can be seen from Fig. 10. For longitudinal slots, such a result has been obtained previously [7]. Fig. 11 shows the value at resonance of $|s_{11}|$ over a frequency range from 8.9 to 10.1 GHz for standard X-band waveguide. For a 50 mil offset slot, $|s_{11}|$ drops 48 percent in this frequency range for $\theta = 0$, whereas it drops 24 percent for $\theta = 20°$. For the larger offset of 250 mil, the drop in $|s_{11}|$ is 39 percent for $\theta = 0°$ and 35 percent for $\theta = 20°$. Again, for large offsets, the θ-dependence of $|s_{11}|$ is not really significant. Similar results were also obtained for reduced height guide. For all offsets and tilts, a very rapid variation in $|s_{11}|$

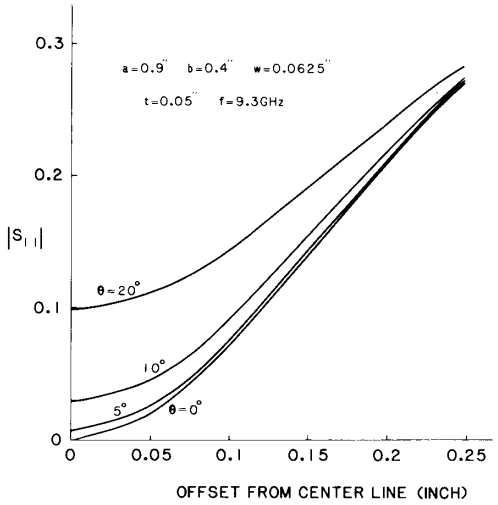

Fig. 9. Magnitude of s_{11} at resonance for compound slots in a standard X-band guide.

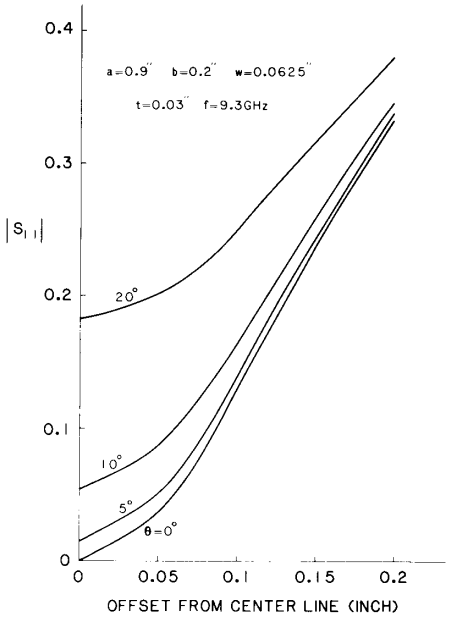

Fig. 10. Magnitude of s_{11} at resonance for compound slots in a half-height guide.

over a frequency range of 13.5 percent was found, as can be seen from Fig. 11. This is due to the fact that $|s_{11}|$ is inversely proportional to $\omega\beta_{10}$ and directly proportional to the aperture electric field. The frequency dependence of $|s_{11}|$ at resonance clearly requires proper consideration in the design of waveguide slot arrays.

C. The Aperture Electric Field

The magnitude of the electric field, $E_{\xi a}$ at the center of the radiating aperture, normalized to the incident TE_{10} mode electric field maximum, is presented in Figs. 12 and 13 for standard X-band waveguide and reduced height guide,

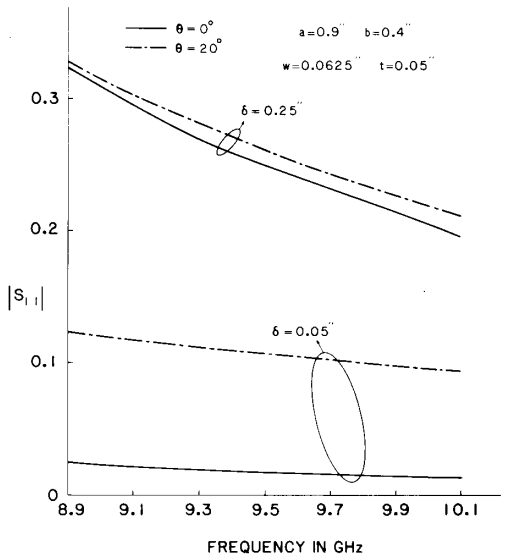

Fig. 11. Magnitude of s_{11} at resonance versus frequency for compound slots in a standard X-band waveguide.

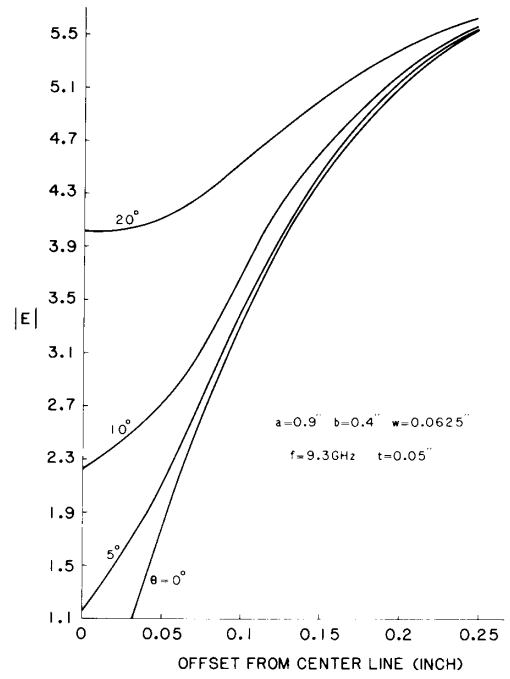

Fig. 12. Magnitude of the aperture electric field at resonance for slots in a standard X-band guide.

respectively. This is the aperture excitation coefficient, an important design parameter for slot arrays. For centered slots, and longitudinal slots, $E_{\xi a}$ is obtained from series and shunt equivalent circuits, respectively. For a compound slot, the equivalent circuit representation is not simple because forward and backward scattering are neither in phase nor out of phase. Hence plots of $E_{\xi a}$ are very useful. These figures also show a rapid variation with θ for small offsets and slow variation for

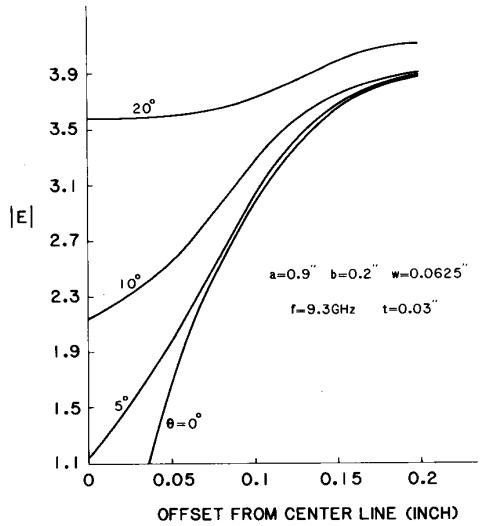

Fig. 13. Magnitude of the aperture electric field at resonance for slots in a half-height guide.

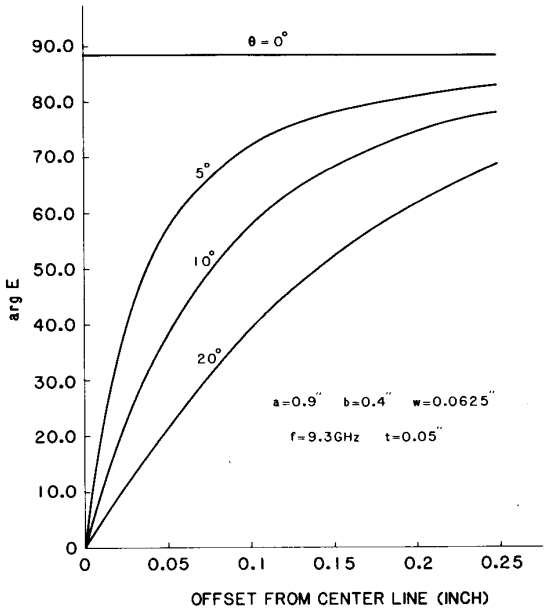

Fig. 14. Phase of the aperture electric field at resonance for slots in a standard X-band guide.

large offsets. Fig. 14 displays the variation of phase of $E_{\xi a}$ (over a 90° range) as a function of offset and tilt. The phase plots are very nearly identical for standard height and half-height guides. Phase variation with θ is rapid for small offsets, and it is less sensitive to θ for large offsets.

The aperture electric field distribution is very nearly a half-cosine distribution, characterized by a dominant contribution from the first Galerkin mode. For large offsets, the first odd term, (the $q = 2$ Galerkin mode) reaches about 5 percent of the $q = 1$ mode amplitude and thus becomes significant. This has the effect of skewing the distribution and is more pronounced for reduced height waveguide. Similar results have been found by Stern and Elliott [7] and Josefsson [13] for

TABLE I
COMPARISON OF THEORY AND EXPERIMENT
a = 0.9 in, b = 0.4 in, w = 0.0625 in, t = 0.05 in, $2l$ = 0.630 in, δ = 0.150 in

	s_{11}	
Tilt	Theory	Experiment
5°	0.161 /172°	0.157 /167°
10°	0.172 /153°	0.168 /151°
20°	0.208 /121°	0.203 /116°

the longitudinal slot. The relative amplitude of the $q = 2$ mode reduces with increasing tilt. Wall thickness has the effect of damping higher order Galerkin mode coefficients due to attenuation of evanescent modes in the short section of waveguide between the two apertures.

A comparison of longitudinal slot characteristics obtained from a previously proven model employing an even electrostatic distribution [7] and those obtained from this work (uniform transverse distribution) shows excellent agreement, for zero wall thickness. The greatest discrepancy between the two models is found for resonant lengths. Even in that case, the deviation is less than 1 percent. For thick wall slots, because of attenuation in higher order modes in the small waveguide, the uniform distribution model should be even better. Similar findings were recently reported for the longitudinal slot by Josefsson [13].

All the results discussed so far were obtained with three expansion modes in the global Galerkin technique. When the number of modes is increased to 15, only the values for resonant length change noticeably. Even this change is of the order of 1.3 percent for zero wall thickness, and for a 30 mil thick wall, the change is less than 0.5 percent. Thus results obtained with three Galerkin modes are quite satisfactory.

D. Comparison of Theory and Experiment

A comparison between s_{11} computed from this theory and that measured experimentally, is made in Table I. The agreement between theory and experiment is seen to be excellent. The small discrepancy in phase corresponds to about 0.5 percent deviation in resonant frequency. It is not clear to what extent it is due to experimental errors, or minor imperfections in this theory.

IV. Conclusion

Integral equations have been developed for a compound radiating slot in the broadwall of a rectangular waveguide, including the effect of finite wall thickness. A novel coordinate transformation and singularity removal technique has been employed in a method of moments analysis. The realizability of an extended range of values for the aperture electric field amplitude and *phase* has been demonstrated. This property of the compound slot makes it versatile in array applications since all elements can be designed to be resonant, leaving slot offset and tilt as the design parameters. For small offsets, the compound slot behaves predominantly like a centered inclined

series element, exhibiting a strong dependence on the tilt. For large offset, it behaves like a shunt element exhibiting a relative insensitivity to tilt. Numerical results obtained for resonant length, aperture electric field, and the forward and backward scattered TE_{10} mode fields in the waveguide, as discussed here, are essential for designing compound slot arrays. Results computed using this theory show excellent agreement with experimental data.

Acknowledgment

The author is grateful to Professor Robert S. Elliott of UCLA for suggesting this problem, and for his continued interest and many helpful discussions throughout the course of this work. Thanks are due to my Hughes colleagues, G. J. Stern, P. K. Park, and L. A. Kurtz for their counsel, and for providing experimental data.

References

[1] B. J. Maxum, "Resonant slots with independent control of amplitude and phase," *IRE Trans. Antennas Propagat.*, vol. AP-8, pp. 384–388, July 1960.

[2] A. F. Stevenson, "Theory of slots in rectangular waveguides," *J. Appl. Phys.*, vol. 19, pp. 24–38, Jan. 1948.

[3] W. H. Watson, *The Physical Principles of Waveguide Transmission and Antenna Systems.* Oxford, England: Clarendon, 1947.

[4] R. S. Elliott, "An improved design procedure for small arrays of shunt slots," *IEEE Trans. Antennas Propagat.*, vol. AP-31, pp. 48–53, Jan. 1983.

[5] T. V. Khac, "A study of some slot discontinuities in rectangular waveguides," Ph.D. dissertation, Monash University, Australia, Nov. 1974.

[6] R. W. Lyon and A. J. Sangster, "Efficient moment method analysis of radiating slots in a thick-walled rectangular waveguide," *Inst. Elec. Eng. Proc.* Pt. H, Microwaves, Opt. and Antennas, vol. 128, no. 4, pp. 197–205, Aug. 1981.

[7] G. J. Stern and R. S. Elliott, "Resonant length of longitudinal slots and validity of circuit representation: Theory and experiment," *IEEE Trans. Antennas Propagat.*, vol. AP-33, no. 11, pp. 1264–1271, Nov. 1985.

[8] R. S. Elliott *et al.*, "The scattering properties of slots cut in the broad wall of a rectangular waveguide," TIC 56B1.30/111 Hughes Missile Syst. Group, Canoga Park, CA, Nov. 1983.

[9] C. T. Tai, *Dyadic Green's Functions in Electromagnetic Theory.* Scranton, PA: in Text, 1971.

[10] ——, "On the eigenfunction expansion of dyadic Green's functions," *Proc. IEEE,* vol. 62, pp. 480–481, 1973.

[11] S. R. Rengarajan, "Analysis of compound radiating slots," Univ. California, Los Angeles, CA, Tech. Rep. 886-001, 1988.

[12] A. A. Oliner, "The impedance properties of narrow radiating slots in the broad face of rectangular waveguide," *IRE Trans. Antennas Propagat.*, vol. AP-5, pp. 1–20, 1957.

[13] L. G. Josefsson, "Analysis of longitudinal slots in rectangular waveguides," *IEEE Trans. Antennas Propagat.*, vol. AP-35, pp. 1351–1357, Dec. 1987.

Sembiam R. Rengarajan (S'77–M'80–SM'85), for a photograph and biography please see page 414 of the March 1988 issue of this TRANSACTIONS.